Materials Research. 2016; 19(5): 1149-1154
DOI: http://dx.doi.org/10.1590/1980-5373-MR-2015-0581

Microwave Absorbing Properties of $NiFe_2O_4$ Nanosheets Synthesized Via a Simple Surfactant-Assisted Solution Route

Chengyun Zhao[a,b], Wei Huang[a], Xianguo Liu[a,b]*, Siu Wing Or[b,c], Caiyun Cui[a,b]

[a] *School of Materials Science and Engineering, Anhui University of Technology, Maanshan 243032, PR China.*
[b] *Department of Electrical Engineering, The Hong Kong Polytechnic University, Hong Kong*
[c] *Hong Kong Branch of National Rail Transit Electrification and Automation Engineering Technology Research Center, Hong Kong*

Received: September 29, 2015; Revised: June 6, 2016; Accepted: August 11, 2016

$NiFe_2O_4$ nanosheets have been synthesized via a simple surfactant-assisted solution route, which are confirmed by X-ray powder diffraction, scanning electron microscopy and transmission electron microscopy. The $NiFe_2O_4$ sample exhibits the sheet-like structure, with width varying from 200 to 800 nm and thickness ranging from 20 to 60 nm. The electromagnetic properties of $NiFe_2O_4$ nanosheets-paraffin composites have been deeply investigated. The multiple dielectric relaxation loss in $NiFe_2O_4$ nanosheets is attributed to the size distribution and morphology of the $NiFe_2O_4$ nanosheets. The magnetic loss in the present system is caused mainly by the natural resonance. An absorber with a thickness of 4.3 mm exhibits an optimal reflection loss (RL) value of -47.1 dB at 7.67 GHz. RL values exceeding -20 dB in the 2.68-17.96 GHz range are obtained by choosing an appropriate absorption-layer thickness between 1.9 and 10 mm. Not only the RL peak frequency but also the number of the peaks can be well explained by the quarter-wavelength cancellation model.

Keywords: *Nanosheets, Ferrites, Transmission electron microscopy, Microwave absorbing materials*

1. Introduction

With the rapid development of microwave shielding technology in solving the electromagnetic (EM) interference pollution problem, huge interests have been focused on EM shielding and absorbing materials. The EM shielding materials cannot eliminate EM wave radically. Therefore, the microwave absorbing materials (MAMs) with the capability of absorbing and attenuating EM energy have become the focus of attention[1-3]. MAMs are generally classified into three types: the resistive loss type, the dielectric loss type and magnetic loss type[4]. Single loss type MAMs limits their application in GHz frequencies due to their intrinsic disadvantages. Among the MAMs, ferrite with the electric and magnetic loss as advantage factor, has been most studied in experiment and applied in both military and civil fields for its large saturation magnetization, superior antioxidation and corrosion resistance, and easy preparation[5]. However, their fatal disadvantages restrict their widespread applications. For example, they have relatively large density (e.g. the density of $NiFe_2O_4$ is about 5 g/cm^3). Compared to their bulk counterparts, the scientific interest on nano-sized ferrite is on the rising, due to their interesting chemistry and physical properties from the size effect and the low density[6].

Spinel nanoferrites (MFe_2O_4: M=Fe, Co, Ni, Mn, Zn, etc) have recently attracted a great deal of attention, due to the broad practical applications in several important fields such as magnetic refrigeration, ferrofluids making, magnetic resonance imaging and high density data storage[7]. Among them, nickel ferrite ($NiFe_2O_4$) is one of the most important spinel ferrites. It is particularly attractive to researchers due to its high magneto crystalline anisotropy, high saturation magnetization and unique magnetic structure[8]. To date, different shaped $NiFe_2O_4$ nanostructures such as fiber, sheet, ribbon, and rod have been synthesized using organic sol-gel technology, porous anodic aluminum oxide templates, mechano chemical method, microemulsion method, etc[9-13].

Snoek pointed that the product of the initial permeability and the resonance frequency was proportional to the saturation magnetization: $(\mu_S\text{-}1)f_r=4\gamma M_S/3$ [6,14]. Because of the precession of magnetization under uniaxial anisotropy filed, both the extent of such precession and the loss of energy are small. In order to solve this problem, planar anisotropy picture has been proposed[6,14,15], which bases on the uniaxial anisotropy. According to the planar anisotropy picture, the amplitude of precession is relatively bigger, which is ascribed to the correction of Snoek's constant with the increase of the ratio ($(\sqrt{H_\theta/H_\phi})$). Larger H_θ with smaller H_ϕ can get higher permeability and higher resonance frequency, where H_θ is the out-of-plane anisotropic field and H_ϕ is the in-plane anisotropy field[14].

The planar anisotropy ferromagnetic particles have been attracting considerable interest in experiment[6]. Herein we report an alternative new wet chemical route to $NiFe_2O_4$ nanosheets in large scale via a simple surfactant-assisted solution route. The $NiFe_2O_4$ nanosheets are believed to exhibit good absorbing properties and potential applications in the microwave absorption fields.

* e-mail: liuxianguohugh@gmail.com

2. Experimental Procedure

2.1 Sample Preparation

All chemicals used were of analytical grade and used as received without further purification. The typical procedure for the as-prepared products was as follows: Under air atmosphere, 8 ml of polyglycol (mw≈400), 0.72 g of $FeSO_4 \cdot 7H_2O$, 0.175g of $NiCl_2 \cdot 6H_2O$, and 1 mL of cyclohexane were in order dissolved in 50 mL of water. After being under ultrasonic radiation for 80 min at room temperature, the above mixture was heated to 70 °C and a solution composed of 20 mL of NH_2-NH_2H_2O (85 wt%) and 0.4 g of NaOH was added. After a reaction for 30 min, the final products were separated by centrifugation, washed five times with water, and dried in vacuum at 60 °C for 5 h.

2.2 Material Characterization

The phase of the as-synthesized products was characterized using X-ray diffraction (Brucker D8 Advance diffractometer) with Cu-K_α radiation (λ = 1.5406 Å). Scanning electron microscopy was performed using JEOL-6300 F SEM at an acceleration voltage of 20 kV. The morphology and size of the products were examined by transmission electron microscopy (JEOL JEM-2100F) at an acceleration voltage of 200 kV.

The $NiFe_2O_4$ nanosheets-paraffin composite was prepared by uniformly mixing $NiFe_2O_4$ nanosheets with paraffin, as described in detail elsewhere, by pressing them into cylinder-shaped compacts[16]. Then the compact was cut into toroidal shape with 7.00 mm outer diameter and 3.04 mm inner diameter. The EM parameters were measured for $NiFe_2O_4$ nanosheets-paraffin composite containing 40 wt% $NiFe_2O_4$ nanosheets, using an Agilent N5244A vector network analyzer. Coaxial method was used to determine the EM parameters of the toroidal samples in a frequency range of 2-18 GHz with a transverse EM mode. The vector network analyzer was calibrated for the full two-port measurement of reflection and transmission at each port. The complex permittivity and complex permeability were calculated from S-parameters tested by the vector network analyzer, using the simulation program of Reflection/Transmission Nicolson-Ross model on the 85071E Materials Measurement Software[16].

3. Results and Discussion

3.1. The phase structure and the morphologies of $NiFe_2O_4$ nanosheets

Figure 1 shows the X-ray diffraction (XRD) pattern of the as-synthesized $NiFe_2O_4$ powders. The powders are considered to be single-phase spinel structure as no extra peaks and no unreacted constituents are observed. These peaks are indexed to the cubic $NiFe_2O_4$ phase according to the standard JCPDS (Card No. 54-0964). The nano-sized nature of the ferrite leads to broadening of the powder XRD peaks. The crystallite size of $NiFe_2O_4$ particles were calculated to be 9.4 nm by using the reflection peak of (311) and Debye-Scherrer's relation.

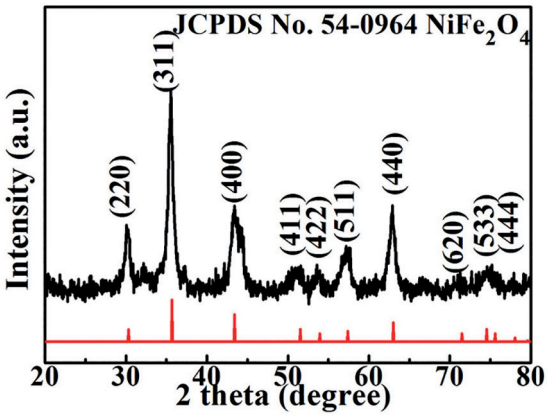

Figure 1: XRD pattern of the as-synthesized $NiFe_2O_4$ powders and the corresponding JCPDS card figure.

The morphology of the $NiFe_2O_4$ powder is analyzed by scanning electron microscopy (SEM) and the image is shown in Figure 2a. Obviously, the powder is composed of nanosheets, with width varying from 200 to 800 nm and thickness ranging from 20 to 60 nm. In Figure 2b, the transmission electron microscopy (TEM) image of the $NiFe_2O_4$ powder further confirms the result of SEM image in Figure 2a. A typical High resolution TEM (HRTEM) image of a nanosheet, as shown in inset of Figure 2b, clearly indicates the d-spacing of 0.481 nm corresponds to the lattice fringe {111} of $NiFe_2O_4$. The $NiFe_2O_4$ powders are identified to be $NiFe_2O_4$ nanosheets.

3.2. Electromagnetic parameters and absorbing performance

Figure 3a and Figure 3b show the complex permittivity (ε_r) and complex permeability (μ_r) versus frequency for the paraffin-based composites containing 40 wt% $NiFe_2O_4$ nanosheets dispersed in a paraffin matrix. In addition, the ε_r and μ_r of the paraffin-based composites are fundamental physical quantities in determining the microwave absorbing properties[17,18]. Figure 3a shows the frequency dependencies of the real part (ε') and the imaginary part (ε'') of the ε_r. Both ε' and ε'' display a similar tendency of decreasing with the frequency increasing from 2 to 18 GHz which is due to increased lagging behind of the dipole-polarization response with respect to the electric-field change at higher frequencies[17]. It is noteworthy that there are multi-nonlinear resonance peaks in the complex permittivity. The appearance of multi-nonlinear resonance peaks may be attributed to

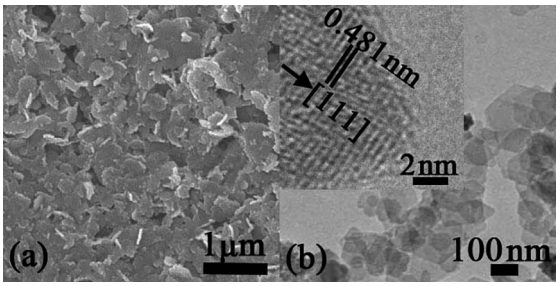

Figure 2: (a) SEM and (b) TEM images of $NiFe_2O_4$ nanosheets. The inset of Fig.2 (b) shows the HRTEM image of $NiFe_2O_4$ nanosheets.

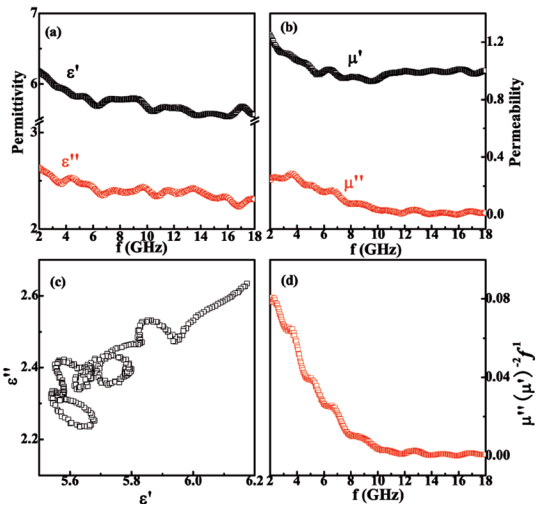

Figure 3: (a) Complex permittivity and (b) permeability, (c) Cole-Cole semicircles and (d) values of $\mu''(\mu')^{-2}f^{-1}$ as a function of frequency for the composite with 40 wt% $NiFe_2O_4$ nanosheets.

the size distribution and the irregular shape of the $NiFe_2O_4$ nanosheets. In addition, the higher-order multipoles of $NiFe_2O_4$ nanosheets and the interaction of inter-nanostructure also introduced multi-resonance peaks[16,19]. From Figure 3b, it can be seen that the real part (μ') of μ_r decreases from 1.24 to 1.00 with frequency increasing. The imaginary part (μ") has a resonance peak at 3.67 GHz, and the large resonance band is observed in the range of 2-10 GHz. The resonance frequency is dependent on the particle's radius, lattice defects and interior stress resulting from the core-shell structure, which can bring a great increase in the effective anisotropy field and further lead to resonance frequency appearing at a different frequency[4]. The large resonance band may be interpreted as a consequence of size and morphology of the $NiFe_2O_4$ nanosheets. Owing to the fact that their length and width is larger than a magnetic wall, $NiFe_2O_4$ nanosheets are made up of several magnetic domains, and the large resonance band may be interpreted as a consequence of their magnetic polydomain configuration. The frequency band broadening is also related to the morphology of the nanostructure because of the effect of the demagnetization fields which are related to the shapes of $NiFe_2O_4$ nanosheets[17].

According to the Debye relaxation theory, for most dynamic processes of dielectric relaxation loss, ε' and ε" follow the equation of the Cole-Cole semicircle. The Cole-Cole semicircles between ε' and ε" for the present system are displayed in Figure 3c.The multi-semicircles are clearly observed in the present system. The multi-semicircles indicate that the multiple dielectric relaxation loss, which is attributed to the size distribution and morphology of the $NiFe_2O_4$ nanosheets. As a typical magnetic material, the magnetic loss of $NiFe_2O_4$ nanosheets is mostly associated with magnetic hysteresis, domain wall resonance, eddy current loss, natural resonance, and exchange resonance for particles smaller than 100 nm[17]. Magnetic hysteresis stemming from irreversible magnetization occurs only in a highly applied field, whereas domain wall resonance derived from multi-domain materials occurs only in the less than GHz frequency range. Exchange resonance should be excluded in the present system, due to the fact that the size of $NiFe_2O_4$ nanosheets is larger than 100 nm. If the magnetic loss only stems from the eddy current loss, then the values of $\mu''(\mu')^{-2}f^{-1}$ should be constant when the frequency is changed. We can call this the skin-effect criterion. As shown in Figure 3d, the values of $\mu''(\mu')^{-2}f^{-1}$ of the $NiFe_2O_4$ nanosheets decrease remarkably with increasing frequency. Therefore, the magnetic loss in the present system is caused mainly by the natural resonance[20].

The reflection loss (RL) of the microwave absorbing material backed on a conductor can be calculated using the ε_r and μ_r at a given frequency and thickness according to the transmit-line theory:

$$RL = 20\lg\left|(Z_{in}-Z_0)/(Z_{in}+Z_0)\right| \quad (1)$$

Where Z_0 is the impedance of free space, and Z_{in} is the input characteristic impedance, which can be express as:

$$Z_{in} = Z_0\sqrt{(\mu_r/\varepsilon_r)}\tanh\{j(2\pi fd/c)\sqrt{\mu_r\varepsilon_r}\} \quad (2)$$

Where c is the velocity of light and d is the thickness of an absorber.

The RL values of the $NiFe_2O_4$ nanosheets are derived according to Eqs. (1) and (2). The three dimensional (3D) dependence of the RL of the $NiFe_2O_4$ nanosheets-paraffin nanocomposites with varying layer thickness (0.6-10 mm) on the frequency in the 2-18 GHz range is presented in Figure 4a. The peak of RL is found to sensitively depend on the thickness. With increasing thickness of the absorption layer, the peak frequency of RL of the $NiFe_2O_4$ nanosheets shifts to lower frequency, and more than one peak of RL appears when the thickness is thicker than a critical value (Figure 4a). An absorber with a thickness of 4.3 mm exhibits an optimal RL value of -47.1 dB at 7.67 GHz. The intensity of the RL peak in Figure 4a first increases, reaches a maximum at 7.67 GHz, and then decreases with the frequency decreasing. The wave energy reflected from the air-air interface is smaller than that from the air-metal interface when frequency is smaller

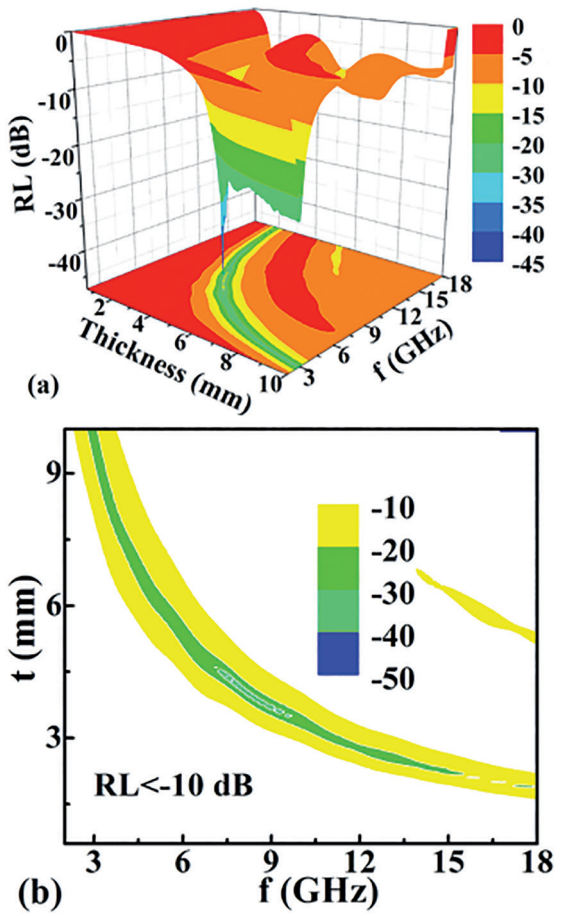

Figure 4: (a) 3D representation of RL as a function of frequency and (b) contour map of the bandwidth with RL<-10 dB (70% absorption) as a function of the absorber thickness.

than the perfect matching frequency (7.67 GHz), and they are going in the opposite direction when frequency is larger than 7.67 GHz[21]. RL values exceeding -20 dB in the 2.68-17.96 GHz range are obtained by choosing an appropriate absorption-layer thickness between 1.9 and 10 mm. This frequency range covers the absorption frequency range of many earlier reported nanocomposites[18-25]. Figure 4b shows the bandwidth of the absorption frequency for RL<-10 dB in a two-dimensional (2D) contour plot. The result indicates that a thicker absorber layer has a wider frequency bandwidth when the thickness is less than 6 mm, and the bandwidth gradually decreases with increasing layer thickness when the thickness is more than 6 mm. The bandwidth of a RL peak is influenced by the derivation of matching thickness to frequency, the matching thickness, the reflected wave energy from air-metal interface, the energy difference of peak frequency, and designated frequency[21].

For the microwave absorbing material backed on a conductor, the peak frequency dependence of the RL complies with the quarter-wavelength cancellation model (QWC): $t_m = nc/4f_m\sqrt{|\varepsilon_r\mu_r|}$ (n = 1,3,….), where f_m is the peak frequency of RL, t_m is the thickness of the absorber. QWC has been successfully used to explain the relationship between RL peak frequency and absorber thickness for flake-shaped carbonyl-iron particle composites, Ni@Ni_2O_3 core-shell particles and hcp-cobalt particles[16,21,26]. Figure 5b gives the dependence of λ/4, 3λ/4 and 5λ/4 on frequency for the $NiFe_2O_4$ nanosheets. The thickness contours at 1.6, 1.9, 2.6, 3.8, 4.3, 5.4, 7.0, 8.0, 9.0 and 10.0 mm, which correspond to the absorber thickness in Figure 5a, are plotted in Figure 5. In Figure 5a, the vertical dot lines are extended from the RL peaks, and each line from the RL peak under an absorber thickness crosses with its corresponding thickness contour in Figure 5b. The crossover points are indicated by the asteroid dots. Since the RL peak comes from the QWC, the frequency and number of RL peak are determined by the QWC condition when the composite thickness is fixed. Furthermore, we can get the following information in 2-18 GHz range from the thickness contours in Figure 5b: (1) when the absorber thickness t<1.66 mm, the thickness contour has no crossover point with the λ/4 curve, indicating no RL peak exists in the RL curve, as shown in Figure 5a at t = 1.6 mm; (2) when 1.66 mm<t<4.98 mm, the thickness contour has one crossover point with the λ/4 curve and one peak should exist in the RL curve; (3) when 4.98 mm< t <8.31 mm, the thickness contour has crossover points with the λ/4 and

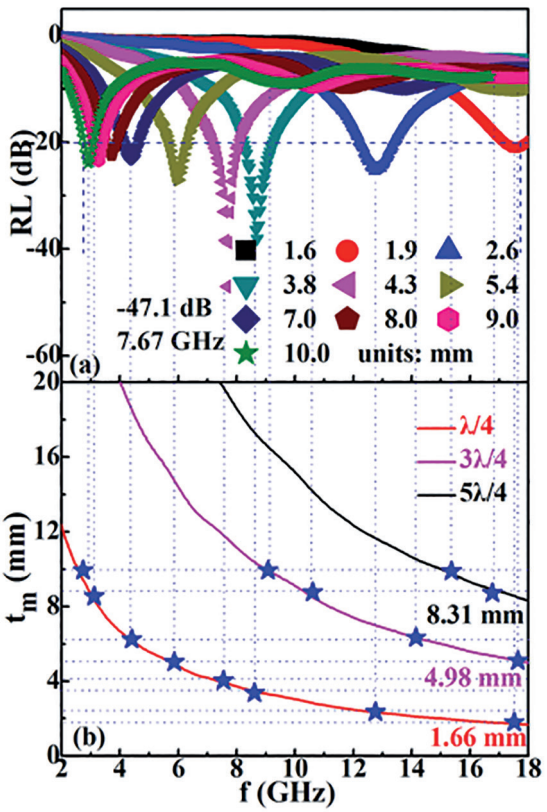

Figure 5: (a) dependence of RL on frequency at various thickness and (b) dependence of λ/4, 3λ/4 and 5λ/4 on frequency for the $NiFe_2O_4$ nanosheets-paraffin composite from its ε_r and μ_r with frequency.

3λ/4 curves, and two peaks should exist in the RL curve, as shown in Figure 5a at t=5.4, 7.0 and 8.0 mm; (4) when t > 8.31 mm, the thickness contour has crossover points with λ/4, 3λ/4 and 5λ/4 curves, and three peaks should exist in the RL curve, which has been verified in the RL curve shown in Figure 5a at 9.0 and 10.0 mm. We can clearly see that all the asteroid dots locate on the λ/4, 3λ/4 and 5λ/4 curves, which demonstrates all the absorber thicknesses are in good agreement with the quarter-wavelength of the composite when the peak appears in the RL curve.

4. Conclusions

In summary, $NiFe_2O_4$ nanosheets, with width varying from 200 to 800 nm and thickness ranging from 20 to 60 nm, have been synthesized in high yield and large-scale via a simple surfactant-assisted solution route. The EM properties of $NiFe_2O_4$ nanosheets-paraffin composites have been deeply investigated. An absorber with a thickness of 4.3 mm exhibits an optimal RL value of -47.1 dB at 7.67 GHz. RL values exceeding -20 dB in the 2.68-17.96 GHz range are obtained by choosing an appropriate absorption-layer thickness between 1.9 and 10 mm. The multiple dielectric relaxation loss in $NiFe_2O_4$ nanosheets is attributed to the size distribution and morphology of the $NiFe_2O_4$ nanosheets. The magnetic loss in the present system is caused mainly by the natural resonance. Considering the low-cost and facile synthesis process of $NiFe_2O_4$ nanostructure with special morphologies, the present study offers promising materials for microwave absorption.

5. Acknowledgements

This study has been supported partly by the National Natural Science Foundation of China (Grant No. 51201002), by the National College Students Innovation and entrepreneurship training program of China (Grant No. 201510360009), and by the Innovation and Technology of the HKSAR Government to the Hong Kong Brach of National Rail Transit Electrification and Automation Engineering Technology Research Center under Grant 1-BBYF.

6. References

1. Zhan J, Yao YL, Zhang CF, Li CJ. Synthesis and microwave absorbing properties of quasione-dimensional mesoporous $NiCo_2O_4$ nanostructure. *Journal of Alloys and Compounds*. 2014;585:240-244.

2. Wu ND, Liu XG, Zhao CY, Cui CY, Xia AL. Effects of particles size on the magnetic and microwave absorption properties of carbon-coated nickel nanocapsules. *Journal of Alloys and Compounds*. 2016;656:628-34.

3. Li MF, Guo JJ, Xu BS. Superelastic carbon spheres under high pressure. *Applied Physics Letters*. 2013;102:121904.

4. Jiang LW, Wang ZH, Li D, Geng DY, Wang Y, An J, et al. Excellent microwave-absorption performances by matched magnetic-dielectric properties in double-shelled Co/C/polyaniline nanocomposites. *RSC Advances*. 2015;5(50):40384-40392.

5. Mehdipour M, Shokrollahi H. Comparison of microwave absorption properties of $SrFe_{12}O_{19}$, $SrFe_{12}O_{19}/NiFe_2O_4$, and $NiFe_2O_4$ particles. *Journal of Applied Physics*. 2013;114:043906.

6. Liu XG, Cui CY, Li TT, Xia AL, Lv YH. Ni@C nanocapsules-decorated $SrFe_{12}O_{19}$ hexagonal nanoflakes for high-frequency microwave absorption. *Journal of Alloys and Compounds*. 2016;678:234-240.

7. Tyagi S, Baskey HB, Agarwala RC, Agarwala V, Shami TC. Synthesis and characterization of $SrFe_{11.2}Zn_{0.8}O_{19}$ nanoparticles for enhanced microwave absorption. *Journal of Electronic Materials*. 2011;40:2004-2014.

8. Sivakumar P, Ramesh R, Ramanand A, Ponnusamy S, Muthamizhchelvan C. Synthesis and characterization of $NiFe_2O_4$ nanoparticles and nanorods. *Journal of Alloys and Compounds*. 2013;563:6-11.

[9. Sivakumar P, Ramesh R, Ramanand A, Ponnusamy S, Muthamizhchelvan C. Preparation and properties of $NiFe_2O_4$ nanowires. *Materials Letters*. 2012;66(1):314-317.

10. Sivakumar P, Ramesh R, Ramanand A, Ponnusamy S, Muthamizhchelvan C. Synthesis, studies and growth mechanism of ferromagnetic $NiFe_2O_4$ nanosheet. *Applied Surface Science*. 2012;258(17):6648-6652.

11. Li FS, Song LJ, Zhou D, Wang T, Wang Y, Wang HB. Fabrication and magnetic properties of $NiFe_2O_4$ nanocrystalline nanotubes. *Journal of Materials Science*. 2007;42(17):7214-7219.

12. Yang HM, Zhang XC, Ao WQ, Qiu GZ. Formation of $NiFe_2O_4$ nanoparticles by mechanochemical reaction. *Materials Research Bulletin*. 2004;39(6):833-837.

13. Sun YP, Liu XG, Feng C, Fan JC, Lv YH, Wang YR, et al. A facile synthesis of $FeNi_3$@C nanowires for electromagnetic wave absorber. *Journal of Alloys and Compounds*. 2014;586:688-692.

14. Qiao L, Han R, Wang T, Tang LY, Li FS. Greatly enhanced microwave absorbing properties of planar anisotropy carbonyl-iron particle composites. *Journal of Magnetism and Magnetic Materials*. 2015;375:100-105.

15. Xue DS, Li FS, Fan XL, Wen FS. Bianisotropy picture of higher permeability at higher frequencies. *Chinese Physics Letters*. 2008;25:4120-4123.

16. Liu XG, Sun YP, Feng C, Jin CG, Li WH. Synthesis, magnetic and electromagnetic properties of Al_2O_3/Fe oxides composite-coated polyhedral Fe core-shell nanoparticles. *Applied Surface Science*. 2013;280:132-137.

17. Wen SL, Liu Y, Zhao XC, Cheng JW, Li H. Synthesis, multi-nonlinear dielectric resonance and electromagnetic absorption properties of hcp-cobalt particles. *Journal of Magnetism and Magnetic Materials*. 2014;354:7-11.

18. Wang H, Guo HH, Dai YY, Geng DY, Han Z, Li D, et al. Optimal electromagnetic-wave absorption by enhanced dipole polarization in Ni/C nanocapsules. *Applied Physics Letters*. 2012;101:083116.

19. Liu XG, Geng DY, Shang PJ, Meng H, Yang F, Li B, et al. Fluorescence and microwave-absorption properties of multi-functional ZnO-coated α-Fe solid-solution nanocapsules. *Journal of Physics D: Applied Physics*. 2008;41(17):175006.

20. Liu XG, Feng C, Or SW, Sun YP, Jin CG, Li WH, et al. Investigation on microwave absorption properties of CuO/Cu_2O-coated Ni nanocapsules as wide-band microwave absorbers. *RSC Advances*. 2013;3(34):14590-4.

21. Wang T, Han R, Tan GG, Wei JQ, Qiao L, Li FS. Reflection loss mechanism of single layer absorber for flake-shaped carbonyl-iron particle composite. *Journal of Applied Physics*. 2012;112:104903.

22. Yan LG, Wang JB, Han XH, Ren Y, Liu QF, Li FS. Enhanced microwave absorption of Fe nanoflakes after coating with SiO_2 nanoshell. *Nanotechnology*. 2010;21(9):095708.

23. Wang H, Dai YY, Gong WJ, Geng DY, Ma S, Li D, et al. Broadband microwave absorption of CoNi@C nanocapsules enhanced by dual dielectric relaxation and multiple magnetic resonances. *Applied Physics Letters*. 2013;102:223113.

24. Liu QL, Zhang D, Fan TX. Electromagnetic wave absorption properties of porous carbon/Co nanocomposites. *Applied Physics Letters*. 2008;93:013110.

25. Pan HS, Cheng XQ, Zhang CH, Gong CH, Yu LG, Zhang JW, et al. Preparation of Fe_2Ni_2N/SiO_2 nanocomposite via a two-step route and investigation of its electromagnetic properties. *Applied Physics Letters*. 2013;102:012410.

26. Wang BC, Zhang JL, Wang T, Qiao L, Li FS. Synthesis and enhanced microwave absorption properties of Ni@Ni_2O_3 core-shell particles. *Journal of Alloys and Compounds*. 2013;567:21-25.